

# The effect of propagation saw test geometries on critical cut length

Bastian Bergfeld<sup>1\*</sup>, Karl W. Birkeland<sup>2</sup>, Valentin Adam<sup>1,3</sup>, Philipp L. Rosendahl<sup>3</sup>, and Alec van Herwijnen<sup>1</sup>

<sup>1</sup> WSL Institute for Snow and Avalanche Research SLF, Davos, Switzerland

<sup>2</sup> Birkeland Snow and Avalanche Scientific, Bozeman, Montana

<sup>3</sup> Institute of Structural Mechanics and Design, Technical University of Darmstadt, Darmstadt, Germany

Correspondence to: Bastian Bergfeld ([bastian.bergfeld@slf.ch](mailto:bastian.bergfeld@slf.ch))

## Abstract:

For a slab avalanche to release, a crack in a weak snow layer beneath a cohesive snow slab has to initiate and propagate. Information on crack propagation is essential for assessing avalanche triggering potential. In the field, this information can be gathered with the Propagation Saw Test (PST), a field test that provides valuable data on crack propagation propensity. The first PSTs were performed about 20 years ago and standards have since been established. However, there are still differences in how the PST is performed. Standards in North America require the column ends to be cut vertically, whereas in Europe they are typically cut normal to the slope. In this study, we investigate the effect of these different column geometries on the critical cut length. To this end, we conducted 27 pairs of PST experiments, each pair consisting of one PST with slope normal cut ends and one PST with vertical cut ends. Our experiments showed that PSTs with normal cut ends have up to 50% shorter critical cut lengths, and the difference predominantly depends on the slope angle and slab thickness. We developed two load-based models to convert critical cut lengths between the test geometries: (i) a uniform slab model that treats the slab as one uniform layer and (ii) a layered model that accounts for stratification. For validation, we compare these models with a modern fracture mechanical model. For the rather uniform slabs of our experiments, both load-based models were in excellent agreement with measured data. For slabs with an artificial layering, the uniform load-model predictions reveal deviations from the fracture mechanical model whereas the layered model was still in excellent agreement. This study reveals the influence that the geometry of field tests and the slope angle of the field site have on test results. It also shows that only accurately prepared field tests can be reliable and therefore meaningful. However, we provide models to correct for imprecise field test geometry effects on the critical cut length.

**KEYWORDS:** stability test, Propagation Saw Test, edge effect, failure initiation

## 1 Introduction

Accurate assessment of fracture initiation and crack propagation is essential to evaluate the potential for triggering avalanches (Schweizer et al., 2016). In this context, the Propagation Saw Test (PST) is a field test that provides valuable insight into the propensity of cracks to propagate (Gauthier and Jamieson, 2006b). In the past 20 years several studies investigated the influence of PST geometry. They aimed to provide recommendations for the PST column length (Bair et al., 2014) or looked into the effect of changing slab thicknesses (Simenhois and Birkeland, 2008). It was also reported that the critical cut length depends on whether the ends of the PSTs are cut slope-normally or vertically (Gaume et al., 2017). Although PSTs have been used for approximately 20 years and utilized in various studies (Bair et al., 2013; Bergfeld et al., 2022; Bergfeld et al., 2021; Birkeland et al., 2019; Gauthier and Jamieson, 2008b), the lack of widely

37 accepted standards hinders its consistent and reproducible application across locations and practitioners. Standards in  
38 North America require the PST column ends to be cut vertically (CAA, 2016; Greene et al., 2022), whereas in Europe  
39 they are typically cut at a normal to the slope (Sigrist and Schweizer, 2007; van Herwijnen et al., 2016).

40 This methodological difference could possibly explain why previous studies were not conclusive as to whether the crit-  
41 ical cut length decreases (Gaume et al., 2017, slope normal cuts) or increases (Gauthier and Jamieson, 2008a; McClung,  
42 2009, both slope vertical cuts) with increasing slope angle. In both, North America and Europe the weak layer is most  
43 commonly cut upslope, but in rare cases, the weak layer is also cut downslope from the top. Gauthier and Jamieson  
44 (2006a) investigated this difference experimentally and observed no significant dependence of critical cut length on cut-  
45 ting direction. However, they also found that critical cut length does not depend on slope angle. Another contradictory  
46 statement about the cut length to slope angle relationship. However, the geometric and/or methodological differences  
47 (column geometry and cutting direction of PSTs) are likely to affect the results of PSTs (Gaume et al., 2017; Heierli et  
48 al., 2008, Supplement Figure S3). Our study aims to investigate the effect of different column geometries and cutting  
49 directions on the critical cut length, a major structural property. To achieve this, we conducted a series of side-by-side  
50 PST experiments with normal and vertical ends. In addition, we also investigated the influence of cutting direction  
51 (upslope or downslope).

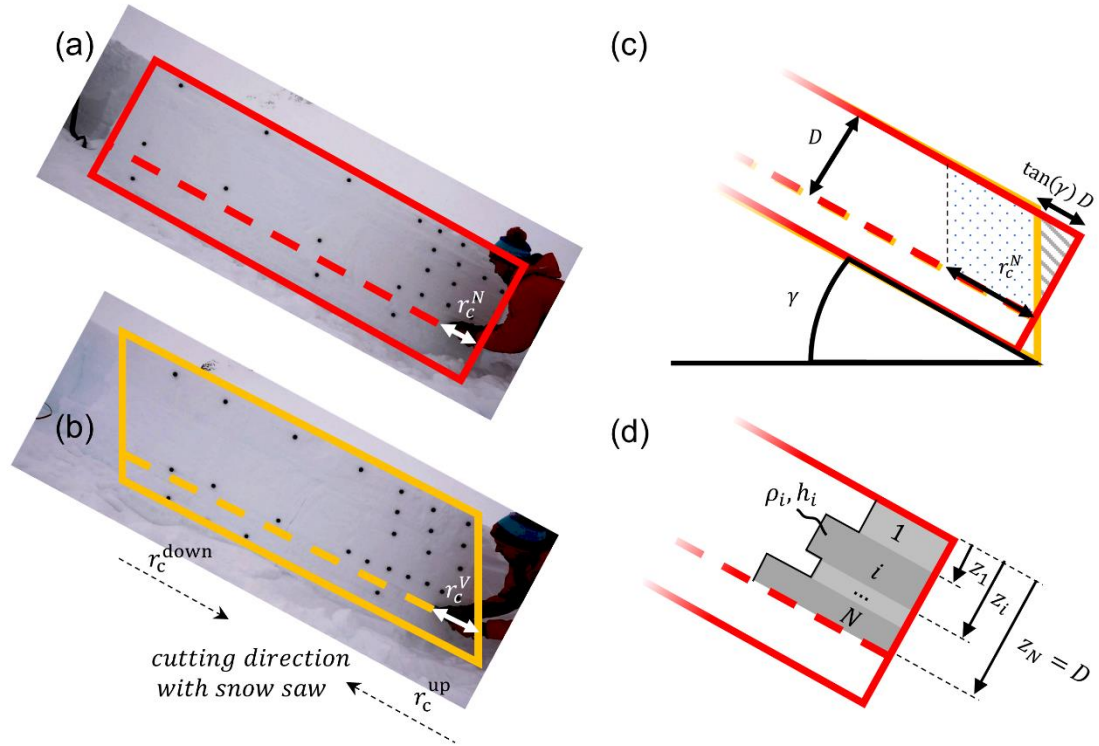
52  
53 The purpose of these experiments was to demonstrate the influence of PST column geometry and cutting direction on the  
54 critical cut length. We also explain where these differences come from and how the stratification of the snowpack influ-  
55 ence these geometric effects. To this end, we developed a uniform- and layered load-based models to convert between  
56 PST geometries. In addition, the developed conversion models were validated against a modern fracture mechanics model  
57 (Rosendahl and Weissgraeber, 2020; Weißgraeber and Rosendahl, 2023).

## 58 2 Methods

### 59 Field Experiments

60 In January and March 2021, we performed field experiments above Davos in the Eastern Swiss Alps, and in Montana,  
61 United States. All field sites were around 2400 m.a.s.l. and PSTs resulted in all possible propagation outcomes (slab  
62 fracture, crack arrest and full propagation). In Davos, we tested a weak layer consisting of surface hoar (grain size: 2-4  
63 mm), while in Montana the weak layer consisted of depth hoar (grain size: 1-4 mm) (Fierz et al., 2008). Slab thickness  
64 ranged from 52 to 96 cm.

65  
66 In total 27 pairs of PSTs were performed, with each pair consisting of one test using slope normal ends (results with  
67 superscript X<sup>N</sup>, [Figure 1Figure 1Figure 1a](#)) and the other with vertical ends (superscript X<sup>V</sup>, [Figure 1Figure 1Figure 1b](#)).  
68 For three pairs, hence for six PSTs, we performed additional PSTs in which the weak layer was cut in downslope direction  
69 immediately next to the PST cut in the upslope direction ( $r_c^{\text{up}}$  and  $r_c^{\text{down}}$  in [Figure 1Figure 1Figure 1b](#)).



70

71

72 **Figure 1:** (a) PST with normal ends and a critical cut length  $r_c^N$ . The red outline indicates the PST geometry. The dashed line indicates the height of the weak layer. (b) PST with vertical ends and a critical cut length  $r_c^V$ . Additionally, the different cutting directions  $r_c^{up}$  and  $r_c^{down}$  are indicated. The two cutting directions were used in both PST geometries. (c) Difference in PST geometry at the downslope end of a PST. The main difference is the additional slab load for the slope normal geometry shown by the grey triangle.  $\tan(\gamma)D$  is the **vertical slope-normal** measured slab thickness and  $\gamma$  the slope angle. (d) In the layered load conversion model, each slab layer  $i$  **(in both the vertical and normal PST configurations)** contributes according to their density  $\rho_i$ , layer thickness  $h_i$  and depth in the slab  $z_i$ .

79 For all PSTs, we recorded the critical cut length as  $r_c^N$  for PSTs with normal ends, and  $r_c^V$  for vertical ends. We then  
 80 compute the ratio of both cut lengths  $r_c^V/r_c^N$ . To investigate the effect of cutting directions, we used the ratio  $r_c^{up}/r_c^{down}$ ,  
 81 where  $r_c^{up}$  and  $r_c^{down}$  indicate whether the critical cut length was taken from upslope or downslope cutting of the weak  
 82 layer, respectively (Figure 1 Figure 1 Figure 1b). Note that the ratio of the cutting direction was determined separately for  
 83 the different PST geometries.

#### 84 Conversion Models

85 Mechanically, **cutting a PST** can be modelled as a cantilever beam **that does not deform sufficiently to come into contact**  
 86 **with the snow under the cut.** The cantilever (unsupported part of the slab) is loaded by the gravitational body forces,  
 87 hence its own mass. This loading has to be carried through a combination of reaction forces (**normal forces,** shear forces,  
 88 and bending moments inside the slab), which all work together to resist the load and maintain the slab's structural integrity.  
 89 The stress transmitted from the slab to the foundation is known as bearing stress or contact stress. As the foundation is  
 90 provided by the intact weak layer, the contact stress is transmitted right ahead of the saw cut. **Generally, the contact stress**  
 91 **has stress intensity close to the saw cut, it fades out away from the saw cut, and has normal and shear stress components.**

92 However, the actual distribution of contact stress is similar in the slope-vertical and slope-normal PST geometry. Simplified, the contact stress is related to a reaction force of the weak layer which supports the cantilever. For a ~~levelled~~ cantilever beam, the ~~vertical-mixed-mode (normal and shear)~~ reaction force  $R$  at the bedding is equal-related to the total load of the unsupported part of the slab:  $R = m g$ , where  $m$  is the total mass of the slab above the saw cut and  $g$  is the gravitational acceleration. The maximum load a weak layer can support before fracture is reached at the critical cut length. Hence, also  $R$  is at a maximum at the critical cut length ( $R_{max}$ ). In our load models, we assume that  $R_{max}$  is specific to a weak layer, which enables us to state that:  $R_{max} = R_{max}^V = R_{max}^N$ , where  $R_{max}^V$  and  $R_{max}^N$  are the reaction forces at the critical cut length which bear the unsupported portion of the slab in the slope-vertical and slope-normal PST geometry, respectively. As the gravitational acceleration is constant, the masses of the unsupported slab of the two PST geometries are equal:

$$102 \quad m^V = m^N \quad (1)$$

103 Note that the mass of the slab above the intact weak layer contributes to  $R_{max}$ , but since these are additive terms which are independent of PST geometry, they cancel each other out in equation 1.

105 **Uniform Load Model (ULM).** If we consider a uniform slab and express the mass  $m$  through snowpack properties equation 1 becomes:

$$107 \quad \rho b r_c^V D = \rho b r_c^N D + \frac{1}{2} \tan(\gamma) D D \rho b \quad (2)$$

108 where  $D$  is the slope normal measured slab thickness,  $\gamma$  the slope angle,  $b$  the PST column thickness and  $\rho$  the slab density (Figure 1 ~~Figure 1~~ ~~Figure 1~~ c). After rearranging, equation 2 results in the following model for the conversion of critical cut lengths (assumption of a uniform slab):

$$111 \quad r_c^V = r_c^N + \frac{\tan(\gamma) D}{2} \quad (3)$$

112 At this point we would like to point out that this relationship (Equation 3) was already suggested in the context of anticrack nucleation. However, the derivation was based purely on geometric considerations and no further verification was carried out (Heierli et al., 2008, Supplement Figure S3).

115 **Layered Load Model (LLM).** The temporal sequence of weather conditions inevitably produces layered slabs in a natural snowpack. The individual layers differ, among other parameters, in their layer thickness and density. A sloped PST with layered slab in slope normal geometry results in more (compared to the ULM) load above the saw cut if high density layers are close to the snow surface (grey triangle in (Figure 1 ~~Figure 1~~ ~~Figure 1~~ c and d). In addition to the slope angle  $\gamma$ , the extra load depends on the individual layer thickness  $h_i$ , density  $\rho_i$ , and on the relative depth  $z_i$  within the slab (Figure 1 ~~Figure 1~~ ~~Figure 1~~ d). Conceptually, the layered load model is based on the same assumptions as the uniform load model. However, it considers the layering which makes the formulation to compute the additional load of PSTs with slope normal geometry more intricate:

$$123 \quad r_c^V = \frac{\sum_{i=1}^N r_c^N h_i \rho_i + \frac{\tan(\gamma)}{2} h_i^2 \rho_i + \tan(\gamma) (z_N - z_i) h_i \rho_i}{\sum_{i=1}^N h_i \rho_i} \quad (4)$$

124 Where  $N$  is the number of layers. Hence for  $N = 1$ , equation 4 simplifies to the ULM (equation 3). For a detailed derivation of the layered load model, see Appendix A.

127 **Layered Mechanical Model (LMM).**

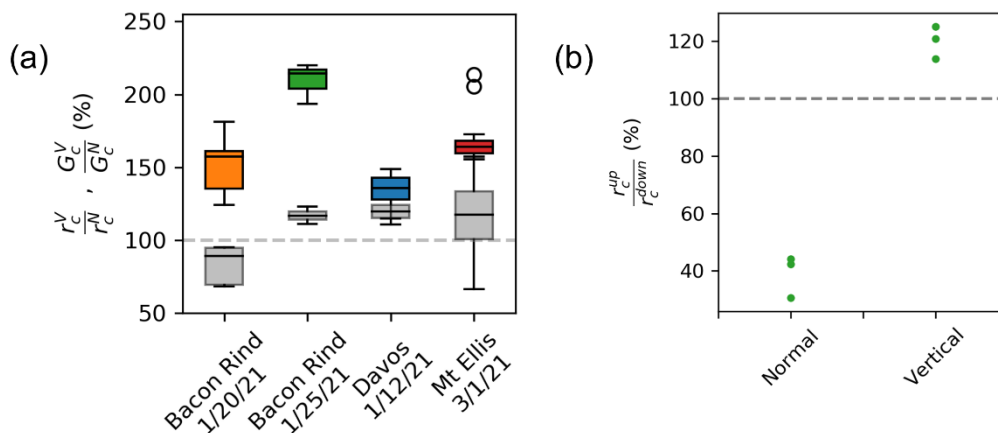
128 For further verification of the load models, we use a closed-form analytical model for layered snowpacks (Weißgraeber  
 129 and Rosendahl, 2023) that was recently validated with field data (Bergfeld et al., 2023), has been utilized. This model  
 130 describes the slab as shear-deformable, layered beam, and allows cylindrical bending, while the weak layer is represented  
 131 as a layer of smeared springs with a Young's and shear modulus. We used the model to determine the critical energy  
 132 release rate  $G_c$  from the measured critical cut length, depending of the geometric configuration ( $G_c^N$  or  $G_c^V$ , respectively).  
 133 This critical energy release rate, also called specific fracture energy, is a material property of the weak layer describing  
 134 its resistance to crack growth, and it is hence a proxy for the fundamental physical process of crack growth in PSTs.  
 135 Subsequently, we used the critical energy release rate determined from an experiment with slope normal beam ends to  
 136 calculate back to the critical cut length of a vertically cut PST. This model is therefore also suitable to convert a critical  
 137 cut length measured in one PST configuration to another. Compared to the ULM (Equation 3) and the LLM (Equation 4),  
 138 the LMM requires many more snowpack properties. However, it represents the specific snowpack layering of a PST and  
 139 its influence on the critical cut length in much more detail, as it takes into account the full deformation behaviour of the  
 140 slab and weak layer system. Uniform slabs or symmetrically (with respect to the centre height of the slab) layered slabs  
 141 are simplifications, usually slabs have a density gradient so that deeper layers have a higher density and are therefore  
 142 stiffer. However, the load models take very little account of the effects of asymmetric slab layering. -We therefore used  
 143 the LMM to verify the influence of an asymmetrically layered slab on our load-based models (ULM, LLM).

## 144 Results

145 In total we performed 66 PSTs at four different field sites. 54 PSTs aimed to investigate the effect of PST geometry  
 146 (Appendix, Table C1), therefore the dataset include 27 pairs of PSTs and each pair consists of one PST with slope normal  
 147 and one with vertical PST beam ends. The remaining 12 PSTs were performed to investigate the difference between  
 148 upslope- and downslope cutting of a PST (Appendix, Table C2).

### 149 Normal vs. vertical PST ends

150 For upslope cutting, critical cut lengths were measured between 14 and 70 cm. Overall,  $r_c^V$  was systematically larger  
 151 than  $r_c^N$ , on average almost 50 % (colored boxes in Figure 2a).



152

153 **Figure 2: (a) Ratio of critical cut lengths shown as boxplots for the different field days (colored). Ratio of the critical energy**  
 154 **release rates computed with the mechanical model using the critical cut lengths of the experiments (grey). Boxes represent the**  
 155 **inter-quartile range with the middle line representing the median value. (b) Ratio of critical cut length from PSTs with**  
 5

156 downslope and upslope cuts. Results are shown for PSTs with normal and vertical PST ends. Both: The dashed line represents  
 157 a ratio of 1.

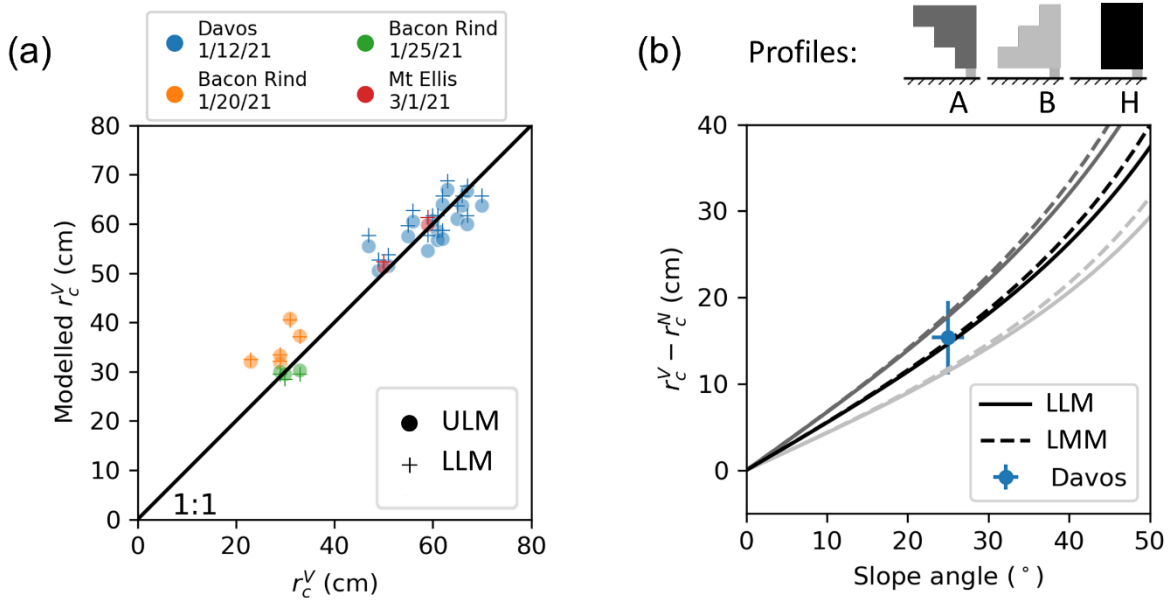
158 Differences in snowpack conditions (e.g. slab thickness, layering, ...) at the various field sites resulted in different devi-  
 159 ations between PST geometries. Median ratios ranged from 136 % to 214 % (Figure 2a, horizontal lines in the colored  
 160 boxes).

161 **Upslope vs. Downslope cutting**

162 Beside PST geometry, the cutting direction also affects the critical cut length. For PSTs with normal ends,  $r_c^{up}$  was about  
 163 40% of  $r_c^{down}$  (Figure 2b, left), while for vertical PST ends  $r_c^{up}$  was about 20% longer than  $r_c^{down}$  (Figure 2b, right).  
 164 Again, these rather large differences can be explained by slab loading and slab mechanics as will be detailed in the dis-  
 165 cussions section.

166 **Models**

167 With Equations (3) and (4) we provide a **uniform load model** and a **layered load model**, respectively. The models allow  
 168 us to convert critical cut lengths between the different PST geometries. Our experiments show very good agreement with  
 169 both the uniform-load model (Figure 3a, dots) and the layered load model (Figure 3a, crosses). The RMSE between the  
 170 measured critical cut lengths in vertical geometry  $r_c^V$  and the modelled counterpart is 4.4 cm for the uniform load model  
 171 and 4.6 cm for the layered load model.



172  
 173 **Figure 3: (a) Modelled critical cut lengths for upslope cuts with vertical PST geometry  $r_c^V$  with the corresponding measured**  
 174 **values, dots represent the uniform load model (ULM, Equation 2) and pluses the layered load model (LLD, Equation 3). Dif-**  
 175 **ferent colors indicate the different field days. The black line is the 1:1 line and indicates a perfect model. (b) Modelled differ-**  
 176 **ences in critical cut lengths with slope angle (upslope cutting). The blue dot represents the mean and uncertainty of the mea-**  
 177 **surements in Davos, as this field day served to define the artificial profiles by matching the mean density. The solid lines are the**  
 178 **layered load model and the dashed lines result from the layered mechanical model (LMM). The grey shades indicate different**  
 179 **slab profiles given at the top of the figure.**

180 Using the **layered mechanical model** to analyse the global energy balance at the onset of crack growth, we derived  
 181 critical energy release rates from the experimental data. The model considers the layering and geometrical configuration  
 182 of a PST experiment to determine the critical energy release rate at the critical cut length, i.e., the specific fracture energy.

183 Unlike the critical cut length, the critical energy release rate is a material property of the weak layer and should thus not  
184 depend on test geometry. In fact, the determined critical energy release rates, measured in the different PST configurations  
185 (vertical or normal beam ends), differed by a maximum of 20% (Figure 2a, grey boxes), whereas the ~~deviations of the~~  
186 critical cut length were up to six times larger (Figure 2a, coloured boxes).

187  
188 Our **uniform load model** considers a homogeneous slab and gives a tangential slope dependence (see Equation 3 and  
189 black solid line in Figure 3b). For comparison, the **layered load model** and the **layered mechanical model** were evaluated  
190 for many different slope angles (Figure 3b, solid and dashed lines, respectively) and 3 different generic slab configurations  
191 (Figure 3b, top). In profile H the mean slab density matched the observed snow cover at our experiments in Davos. The  
192 direct comparison for the artificial profile H shows a very good agreement between the load models and the mechanical  
193 model (compare black solid line and black dashed line in Figure 3b). Note that for profile H the two load models are  
194 equal. The deviations of the critical cut lengths ( $r_c^V - r_c^N$ ) measured in Davos can be reproduced very accurately with all  
195 models (Figure 3b, black lines and blue dot). In the asymmetric profiles A and B, additional artificial layers with the  
196 minimum and maximum density of the Davos snow profile were inserted. For these highly asymmetric slabs (grey lines  
197 in Figure 3) there are deviations between the models. Of course, the uniform model cannot represent any differences  
198 induced by the layering. However, the layered load model and the mechanical model show good agreement over the entire  
199 angle range, whereby the deviations slightly increase with increasing slope angles.

## 200 **Discussion**

### 201 **Normal vs. vertical PST ends**

202 PSTs with slope-normal and vertical ends showed large differences in the measured critical cut length. These differences  
203 can be explained with the different PST geometries and the corresponding slab-induced loading of the weak layer. We  
204 assume that PST beams were long enough, so that the tail end of the PST beam remains mechanically unchanged when  
205 the saw cut is increased and is therefore not relevant (Bair et al., 2014). The constellation is as shown schematically in  
206 Figure 1c. Even with no saw cut, the slope normal PST geometry already has an "unsupported" portion of the slab above  
207 the weak layer (Figure 4a, blue area at the right beam end). This additional load, in normal geometry, generates higher  
208 stresses in the weak layer (and higher energy release rate), leading to shorter critical cut lengths. The shorter critical cut  
209 lengths can therefore easily be attributed to this additional load. However, the extent of the difference depends on snow-  
210 pack properties (e.g. slab thickness, density layering) and slope angle.

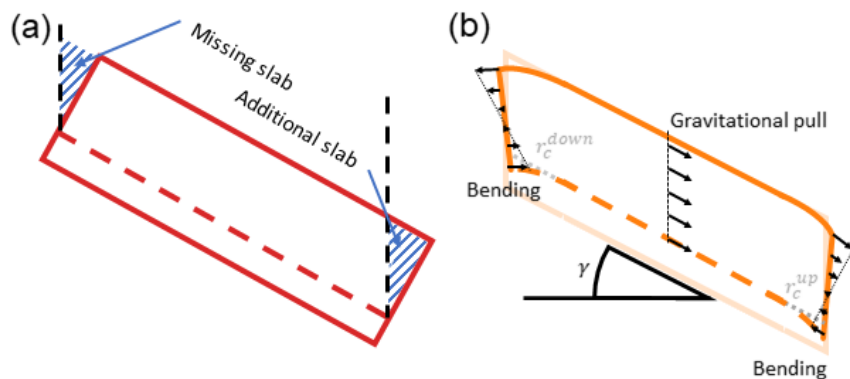
211  
212 This emphasizes that a measured critical cut length can only be interpreted for stability assessment if the applied geometric  
213 PST configuration (including slope angle) is considered. In other words, our data show that two equal snowpacks, which  
214 should exhibit a similar crack propagation propensity, likely result in completely different critical cut lengths depending  
215 on how the PST beam ends were cut and on which slope angle the PST was performed. To ensure comparability of  
216 measured critical cut lengths, it is thus imperative to account for the geometrical configuration and snowpack layering,  
217 using the models presented.

218 **Upslope vs. Downslope cutting**

219 When cutting upslope, there is an additional part of the slab that induces an extra load on the weak layer in the slope  
220 normal configuration (Figure 4a, blue area at the right beam end). When cutting from the top, however, a part of the slab  
221 is missing, and there is less load (Figure 4a, blue area at the left beam end). The critical cut length of the upslope cut is  
222 thus much shorter, in our experiments about 60% shorter (left side in Figure 2b).

223  
224 In the vertical configuration, on the other hand, the load over the saw cut is always the same, independent of the cutting  
225 direction. The observed differences, however, come from the differences in shear stress at the crack tip. Indeed, at the  
226 weak layer, there are two shear stress components: (i) shear stress from the slope parallel gravitational pull on the slab  
227 (Figure 4b, arrows in the middle), and (ii) bending induced shear stresses (Figure 4b, arrows at the left and right beam  
228 end). The slope parallel gravitational pull is always in the same direction (downslope). The bending induced shear stresses  
229 at the height of the weak layer, on the other hand, are always in the cut direction. When cutting the weak layer from the  
230 bottom upwards, both contributions thus have an opposite effect and partially cancel each other out, while when cutting  
231 from the top, both shear stresses have the same sign and add up. This results in longer critical cut lengths when sawing  
232 upslope in vertical PSTs. In our measurements, these were 20% longer (right side in Figure 2b).

233



234

235 **Figure 4:** (a) Schematic representation of a PST with normal ends and without a saw cut. The blue marked areas, at the right  
236 and left of the PST beam, indicate the additional and missing slab load, respectively, relative to vertical ends (black dashed  
237 lines). (b) PST with vertical ends and critical cut lengths  $r_c^{up}$  and  $r_c^{down}$  for upslope and downslope cutting, respectively. At  
238 both PST beam ends the saw cut leads to bending, which results in a stress profile across the slab thickness (black arrows). In  
239 the middle part of the PST, the black arrows represent stress in the slab due to the slope parallel gravitational pull.  $\gamma$  is the  
240 slope angle.

241

242 **Models**

243 Overall, the load models effectively explained our field results. (Figure 3a). If the RMSE of the uniform load- and layered  
244 load model is compared, the uniform load model performs slightly better than the layered load model. However, since  
245 our snowpack profiles show relatively homogeneous slabs without pronounced asymmetry (see Appendix D), we would  
246 not attach any significance to this minor difference, especially for inhomogeneous and asymmetrical slabs. We believe  
247 the layered load model is more accurate. This becomes clear in Figure 3b. Profiles A and B have a density gradient  
248 within the slab (asymmetry). Deviations between the uniform and the layered load model seem plausible as higher density  
249 layers which are close to the snow surface contribute more to the additional load present in slope normal PSTs (blue



250 hashed in Figure 4a) than if they are deeper in the snowpack. The difference in critical cut lengths is expected to be larger  
251 (profile A) or smaller (profile B) than predicted by the uniform load model.

252

253 Beside the overall good conversion performance of the models, a systematic offset for PSTs from 20 January 2021 seem  
254 to be present (orange dots in Figure 3). We suspect that in these PSTs the beam length was too short, the ratio between  
255 slab thickness and beam length was only about 0.5 and the cut length to beam length ratio was 0.25. It is therefore very  
256 likely that the geometric difference at the tail end of the beam was also relevant (Bair et al., 2014). However, this is not  
257 considered in the models. Overall, our results thus show that the PST geometry plays an important role in the measured  
258 critical cut length, and this is mostly driven by differences in load from the slab.

259

### 260 **Model application and limitation:**

261 PST datasets with different PST configurations can be homogenised using our models. This will increase the compara-  
262 bility and ultimately the scientific utility of these datasets. In addition, it is often the case that the PST ends are cut  
263 imprecisely (not perfectly vertical or slope normal) on inclined terrain. The angle of the free edge can easily be determined  
264 from photos of the test, and a correction can then be applied using one of the load models with minor modifications  
265 (Appendix B). The scatter of the experimentally determined critical cut lengths should thus be reduced.

266 Beside applications, shortcomings of the suggested load models are evident. Although, our experimental results show  
267 that the relationship is sufficiently accurate for the conversion of PST geometries, additional changes (e.g. a different  
268 slope angles lead to different contributions of normal and shear loading of the weak layer, which may alter the critical  
269 loading a weak layer can withstand. Ultimately, also influencing measured critical cut lengths) beyond the PST ~~geome-~~  
270 ~~try are geometry are~~ directly affecting model performance, so the relationship may no longer be sufficient. Imagine addi-  
271 tional terms from factors  $A$  and contributions  $B$  in Equation 1:

$$272 A(\gamma, H^N D, \dots) m^V + B(\gamma, H^N D, \dots) \propto A(\tilde{\gamma}, \tilde{D} \tilde{H}^N, \dots) m^N + B(\tilde{\gamma}, \tilde{D} \tilde{H}^N, \dots)$$

273 Both can have functional relationships on properties such as slope angle ( $\gamma, \tilde{\gamma}$ ) and slab thickness ( $D H^N, \tilde{D} \tilde{H}^N$ ).

274 As long as such properties remain unchanged ( $\gamma = \tilde{\gamma}, H^N D = \tilde{D}$ ), the additional terms cancel each other out and our load  
275 models are applicable.

276 However, if the critical cut length measured at a certain slope angle and snow cover has to be transferred to a different  
277 situation, the applicability of our models still needs to be confirmed with more experimental work. If necessary, the  
278 functional relationships  $A$  and  $B$  will probably have to be identified and added. A more generally valid conversion for  
279 critical cut lengths would be of great practical benefit as it allows to extrapolate measured point information on crack  
280 propagation propensity to other slope areas where experimental work is not possible.

### 281 **Conclusion and Outlook**

282 This work has shown that the result of a PST, i.e., the measured critical cut length, is strongly influenced by the test  
283 geometry and cutting direction. PSTs with slope normal beam ends (upslope cutting) systematically produce shorter crit-  
284 ical cut lengths (48% on average). It also makes a significant difference whether the saw cut in a PST is made in the  
285 upslope or downslope direction (deviations up to 60%). Both deviations can be explained mechanically and are largely  
286 controlled by the difference in slab induced loads. Based on the slab load, a load model was derived for uniform, as well  
287 as for layered slabs. Both models agree well with the experimental results. The comparison with a more sophisticated

288 validated fracture mechanical model shows good agreement between all models as long as the slab is largely homogene-  
289 ous. For layered slabs, the uniform load model shows greater deviations. The layered load model, on the other hand,  
290 shows only minor deviations. This demonstrates that the fracture mechanical model (LMM) is also largely load-driven in  
291 this specific application. Overall, our results show that the interpretation of measured critical cut length in a PST is not  
292 straightforward, as it is influenced by weak layer properties (specific fracture energy), slab properties (e.g. layering), and  
293 test geometry.

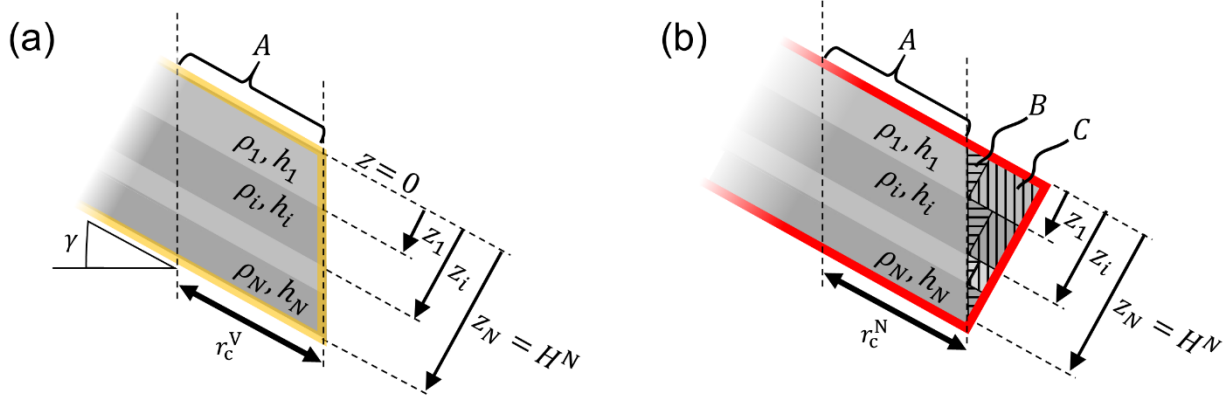
294  
295 Based on our findings, we show that PSTs with slope normal ends and a saw cut in upslope direction (Figure 1a) lead to  
296 the shortest critical cut lengths. Hence, this procedure gives us the most conservative information on crack propagation  
297 propensity (without post-processing). In addition, shorter critical cut lengths ensure that the overall column length is less  
298 likely to influence test result. However, the disadvantage of this approach is the greater effect of slope angle on critical  
299 cut lengths than for vertically cut PSTs. In order to compare tests on different slopes, this effect must be compensated for,  
300 which is not yet straight forward. For an unbiased interpretation of PST results, experiments therefore need to be post-  
301 processed before results from different snow packs, slope inclinations, etc. are compared or combined.

302  
303 In general, the use of consistent PST standards will ensure that PST results are easy to interpret, will ensure scientific  
304 rigor and will improve the comparability of tests and their results. In addition, standardization and conversion models  
305 facilitate the comparison of results between researchers, leading to a deeper understanding of snowpack behavior. Prac-  
306 titioners also benefit from standardized methods and interpretation aids that are invaluable in assessing avalanche risk  
307 based on stability tests.

#### 308 309 **Appendix A:**

310 The load above the saw cut of a PST with slope vertical geometry (V-PST) is independent of the slope angle. However,  
311 the load of a PST with slope normal edges (N-PST) is not. In sloped terrain, a N-PST has more load above the saw cut  
312 than a V-PST. The difference depends on the slope angle, but the layering also has an influence. Layers close to the snow  
313 surface contribute more to the extra load than layers close to the weak layer (of the saw cut). In order to express the  
314 relationship between critical cut lengths ( $r_c^V, r_c^N$ ) the loads of layered snowpacks ( $m^V, m^N$ ) have to be formulated through  
315 density  $\rho_i$ , thickness  $h_i$  and the vertical location  $z_i$  of the slab layers  $i$  (Figure A1).

316



317

318 **Figure A1: (a) Schematic representation of a layered slab in a PST with slope vertical geometry (V-PST). (b) PST with slope**  
 319 **normal geometry (N-PST). In both cases, “A” indicates the volume of the slab above the saw cut  $r_c^x$ . The mass of volume A**  
 320 **depends on column width  $b$  (not indicated), on  $r_c^x$  as well as the density  $\rho_i$  and thickness  $h_i$  of the slab layers  $i$ . In (b), the load**  
 321 **of the N-PST depends additionally on the slope angle as the Volumes B and C of each layer  $i$  increase with increasing angle.**

322 First for the simpler case of a V-PST (Figure A1a) the mass  $m^V$  is given by:

$$323 \quad m^V = m_A = r_c^V b \sum_{i=1}^N h_i \rho_i \quad (A1)$$

324 In the N-PST the Volumes B and C also contribute to the overall mass located above the saw cut:

$$325 \quad m^N = m_A + m_B + m_C \quad (A2)$$

326 The expression for the mass of Volume A remains the same as given in Equation A1. Now, however, the critical crack  
 327 length  $r_c^N$  is relevant instead of  $r_c^V$ . The masses  $m_B$  and  $m_C$  are given by:

$$328 \quad m_B = \frac{1}{2} h_1^2 \tan(\gamma) b \rho_1 + \frac{1}{2} h_2^2 \tan(\gamma) b \rho_2 + \dots + \frac{1}{2} h_N^2 \tan(\gamma) b \rho_N = \frac{b \tan(\gamma) \sum_{i=1}^N h_i^2 \rho_i}{2} \quad (A3)$$

$$329 \quad m_C = (z_N - z_1) \tan(\gamma) h_1 b \rho_1 + (z_N - z_2) \tan(\gamma) h_2 b \rho_2 + \dots + (z_N - z_N) \tan(\gamma) h_N b \rho_N$$

$$330 \quad = b \tan(\gamma) \sum_{i=1}^N (z_N - z_i) h_i \rho_i \quad (A5)$$

331 Putting this together results in the overall mass of:

$$332 \quad m^N = \tan(\gamma) b r_c^N \sum_{i=1}^N \frac{h_i \rho_i}{\tan(\gamma)} + \frac{h_i^2 \rho_i}{2 r_c^N} + \frac{(z_N - z_i) h_i \rho_i}{r_c^N} \quad (A4)$$

333

334 Inserting in Equation A1 results in the layered load model providing the relation between the critical cut lengths  $r_c^V$  and  
 335  $r_c^N$ :

336

$$337 \quad r_c^V = r_c^N \frac{\tan(\gamma) \sum_{i=1}^N \frac{h_i \rho_i}{\tan(\gamma)} + \frac{h_i^2 \rho_i}{2 r_c^N} + \frac{(z_N - z_i) h_i \rho_i}{r_c^N}}{\sum_{i=1}^N h_i \rho_i}$$

$$338 \quad = \frac{\sum_{i=1}^N r_c^N h_i \rho_i + \frac{\tan(\gamma)}{2} h_i^2 \rho_i + \tan(\gamma) (z_N - z_i) h_i \rho_i}{\sum_{i=1}^N h_i \rho_i} \quad (A5)$$

339

340 **Appendix B:**

341 The equations derived in appendix A can be used to formulate a model to correct for imprecisely cut PST beam ends. E.g.  
 342 the sawing edge of a PST was close to cut slope normal, but with a deviation of angle  $\beta$  from slope normal (or vertical).

343 As a result, the critical cut length  $r_c^{\bar{N}}$  is measured in such an experiment. To account for this deviation, we have to add a  
 344 mass  $m_D$  in Equation A2. Note that this “mass” can be negative in the case  $\beta$  is negative (less overhanging mass than the  
 345 slope normal cut). The mass  $m_D$  has the same contributions as  $m_B$  and  $m_C$  but is computed from the angle of error  $\beta$ :

$$346 \quad m_D = \frac{b \tan(\beta) \sum_{i=1}^N h_i^2 \rho_i}{2} + b \tan(\beta) \sum_{i=1}^N (z_N - z_i) h_i \rho_i \quad (\text{B1})$$

347 At the end, the loads (Equation 1) provide the relation between the critical cut lengths:

348

349

$$350 \quad m_A(r_c^{\bar{N}}) + m_B + m_C + m_D = m_A(r_c^N) + m_B + m_C$$

351

$$352 \quad \Rightarrow m_A(r_c^N) = m_A(r_c^{\bar{N}}) + m_D \quad (\text{B2})$$

353 By inserting the formulations for  $m_A$  (equation A1), the formula to correct an imprecisely cut N-PST is derived as:

$$354 \quad r_c^N = \frac{r_c^{\bar{N}} b \sum_{i=1}^N h_i \rho_i + b \tan(\beta) \sum_{i=1}^N \frac{h_i^2 \rho_i}{2} + (z_N - z_i) h_i \rho_i}{b \sum_{i=1}^N h_i \rho_i}$$

$$355 \quad = r_c^{\bar{N}} + \frac{\tan(\beta) \sum_{i=1}^N \frac{h_i^2 \rho_i}{2} + (z_N - z_i) h_i \rho_i}{\sum_{i=1}^N h_i \rho_i} \quad (\text{B3})$$

356

357 **Appendix C:**

358 **Table C1: Results of 27 pairs of PSTs, critical cut lengths  $r_c^V$  and  $r_c^N$  indicate whether PST beam ends were cut vertical or slope**  
 359 **normal. Slab thickness  $H^N$  was measured in slope normal direction. Slope angle is provided in degrees. For further snowpack**  
 360 **data we refer to the Appendix D.**

PST- pairs	Location Date	Critical cut length $r_c^V$ (cm)	Critical cut length $r_c^N$ (cm)	Slab thickness $H^N$ (cm)	Slope angle (°)
1	Davos 1.12.21	55 (±2)	43 (±2)	62 (±2)	25 (±2)
2	Davos 1.12.21	49 (±2)	36 (±2)	62 (±2)	25 (±2)
3	Davos 1.12.21	47 (±2)	41 (±2)	62 (±2)	25 (±2)
4	Davos 1.12.21	51 (±2)	37 (±2)	62 (±2)	25 (±2)
5	Davos 1.12.21	56 (±2)	46 (±2)	62 (±2)	25 (±2)
6	Davos 1.12.21	61 (±2)	45 (±2)	58 (±2)	25 (±2)
7	Davos 1.12.21	59 (±2)	41 (±2)	58 (±2)	25 (±2)
8	Davos 1.12.21	65 (±2)	47 (±2)	60 (±2)	25 (±2)
9	Davos 1.12.21	66 (±2)	49 (±2)	63 (±2)	25 (±2)
10	Davos 1.12.21	70 (±2)	49 (±2)	63 (±2)	25 (±2)
11	Davos 1.12.21	61 (±2)	42 (±2)	63 (±2)	25 (±2)
12	Davos 1.12.21	63 (±2)	52 (±2)	64 (±2)	25 (±2)
13	Davos 1.12.21	62 (±2)	42 (±2)	64 (±2)	25 (±2)
14	Davos 1.12.21	62 (±2)	49 (±2)	64 (±2)	25 (±2)
15	Davos 1.12.21	67 (±2)	45 (±2)	64 (±2)	25 (±2)
16	Davos 1.12.21	67 (±2)	51 (±2)	67 (±2)	25 (±2)
17	Davos 1.12.21	60 (±2)	45 (±2)	67 (±2)	25 (±2)
18	Bacon Rind 1.20.21	31 (±2)	25 (±2)	57 (±2)	29 (±2)
19	Bacon Rind 1.20.21	33 (±2)	21 (±2)	56 (±2)	30 (±2)
20	Bacon Rind 1.20.21	29 (±2)	16 (±2)	55 (±2)	30 (±2)
21	Bacon Rind 1.20.21	29 (±2)	18 (±2)	55 (±2)	29 (±2)
22	Bacon Rind 1.20.21	23 (±2)	17 (±2)	54 (±2)	29 (±2)
23	Bacon Rind 1.25.21	29 (±2)	15 (±2)	52 (±2)	30 (±2)
24	Bacon Rind 1.25.21	33 (±2)	15 (±2)	53 (±2)	30 (±2)
25	Bacon Rind 1.25.21	30 (±2)	14 (±2)	54 (±2)	30 (±2)
26	Mount Ellis 3.1.21	59 (±2)	38 (±2)	93 (±2)	25 (±2)
27	Mount Ellis 3.1.21	50 (±2)	29 (±2)	95 (±2)	25 (±2)

361

362

363 **Table C2: Critical cut lengths measured at Mount Ellis, Critical cut lengths  $r_c^{\text{DOWN}}$  and  $r_c^{\text{UP}}$  indicate if the weak layer was cut**  
 364 **downslope or upslope, respectively. Slab thickness  $H^N$  was measured in slope normal direction. Slope angle is provided in de-**  
 365 **grees. For further snowpack data we refer to the Appendix D.**

366

PST-pairs	Location Date	PST Geometry	Critical cut length $r_c^{\text{DOWN}}$ (cm)	Critical cut length $r_c^{\text{UP}}$ (cm)	Slab thickness $H^N$ (cm)	Slope angle (°)
1	Bacon Rind 1.25.21	Slope normal	49 ( $\pm 2$ )	15 ( $\pm 2$ )	50 ( $\pm 2$ )	30 ( $\pm 2$ )
2	Bacon Rind 1.25.21	Vertical	24 ( $\pm 2$ )	29 ( $\pm 2$ )	52 ( $\pm 2$ )	30 ( $\pm 2$ )
3	Bacon Rind 1.25.21	Slope normal	29 ( $\pm 2$ )	33 ( $\pm 2$ )	54 ( $\pm 2$ )	30 ( $\pm 2$ )
4	Bacon Rind 1.25.21	Vertical	50 ( $\pm 2$ )	50 ( $\pm 2$ )	53 ( $\pm 2$ )	30 ( $\pm 2$ )
5	Bacon Rind 1.25.21	Slope normal	33 ( $\pm 2$ )	14 ( $\pm 2$ )	53 ( $\pm 2$ )	30 ( $\pm 2$ )
6	Bacon Rind 1.25.21	Vertical	24 ( $\pm 2$ )	30 ( $\pm 2$ )	53 ( $\pm 2$ )	31 ( $\pm 2$ )

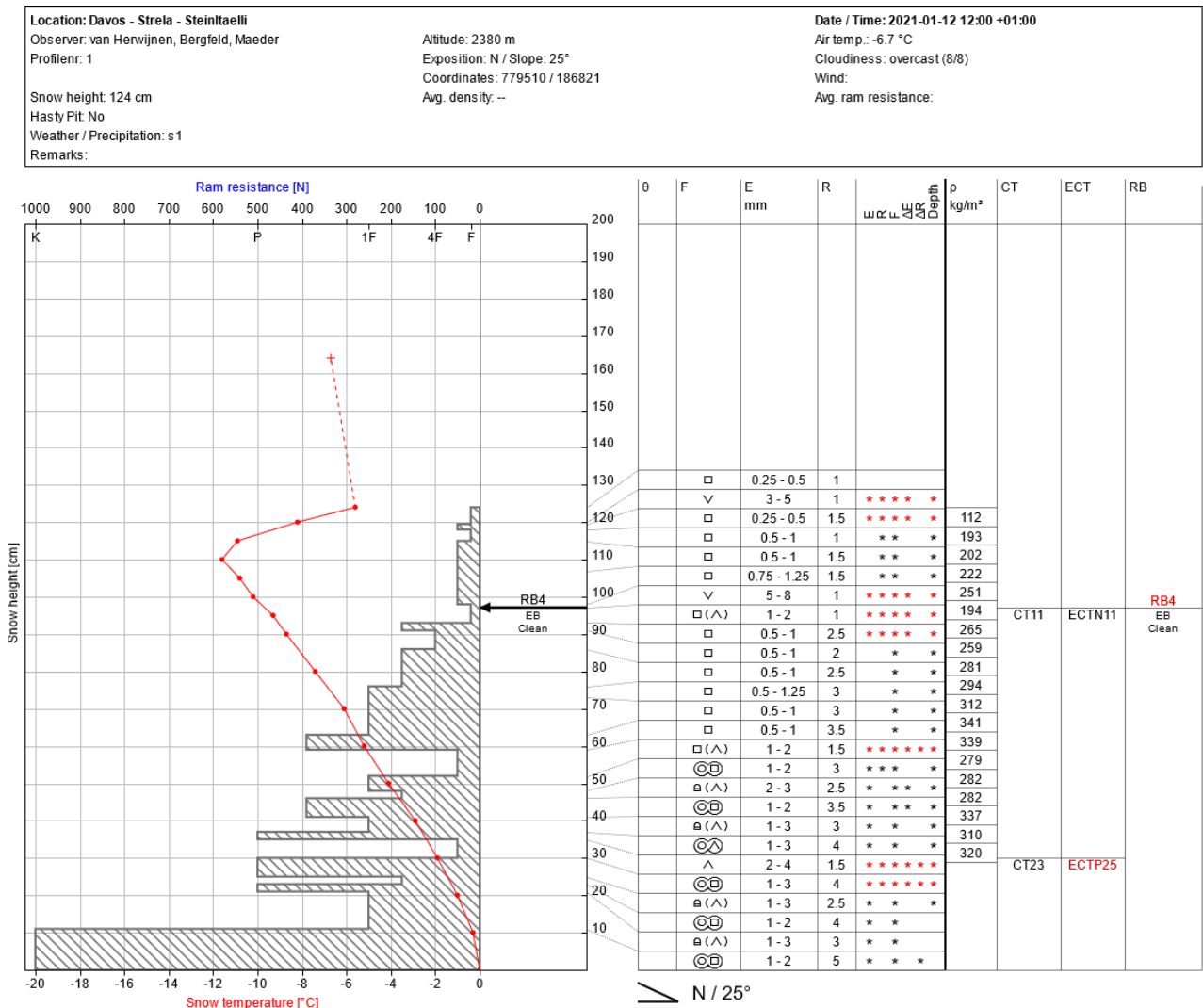
367

368

369 **Appendix D:**

370 At each of our four field sites we took a manual profile including density measures. The following four figures are excerpts  
 371 from the corresponding snow profile databanks.

372



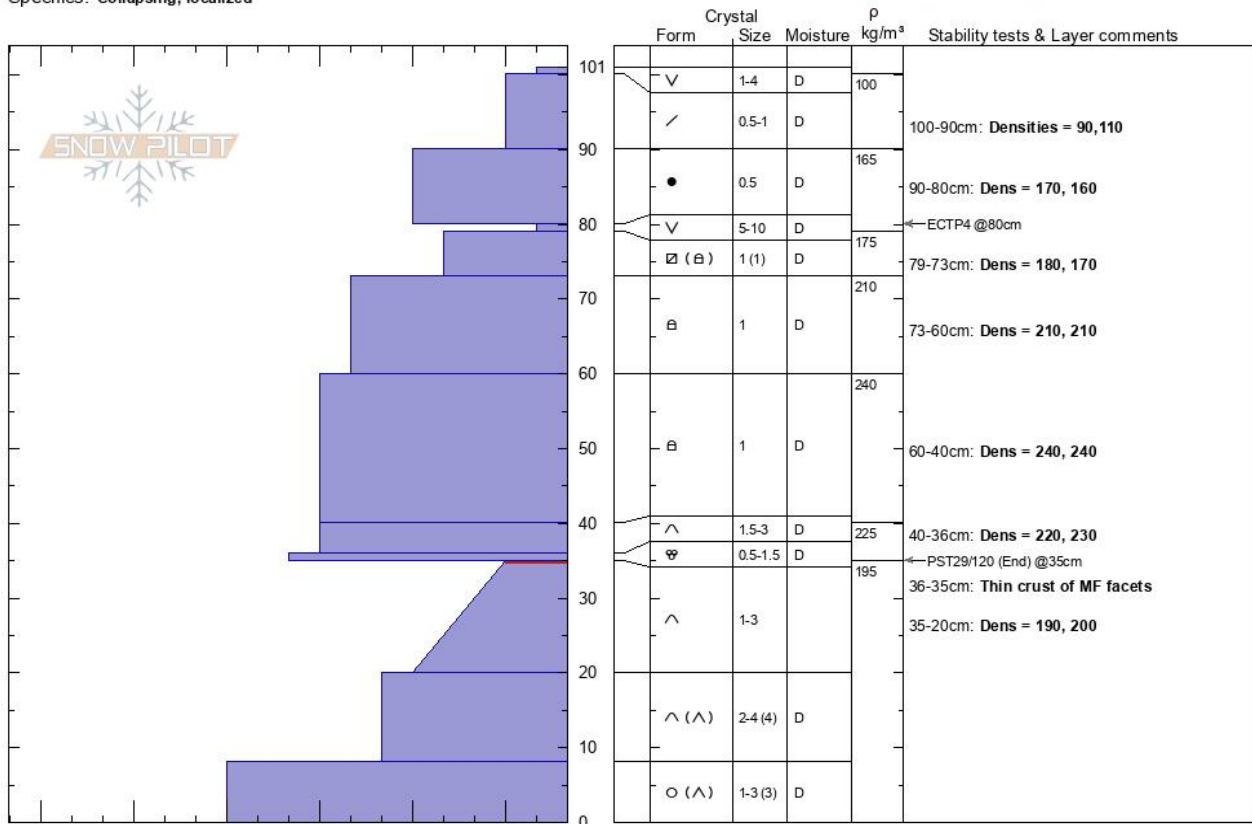
373

374 **Figure D1: Manual profile taken at the Davos field site. The hashed area at the left site represents the hand hardness with snow**  
 375 **height, the red line snow temperature with snow height. On the right side, grain type, grain size, hand harness, lemons and**  
 376 **snow density are given. On the very right, stability test results are written at the height, of the tested weak layer.**

**Bacon Rind Sm Meadow Karl Birkeland**  
**Bridger Range 01/20/2021 - 12:00pm**  
**MT Co-ord: 44.88192N, -111.07457W**  
 Elevation: 2315 m Slope Angle: 30°  
 Aspect: 90° Wind Loading: no  
 Specifics: Collapsing, localized

Stability:  
 Air Temperature:  
 Sky Cover: CLR  
 Precipitation: NO  
 Wind: Calm

HS: 101 Layer Notes:  
 PF: 90 100-90cm: Densities = 90,110  
 90-80cm: Dens = 170, 160  
 79-73cm: Dens = 180, 170  
 73-60cm: Dens = 210, 210  
 60-40cm: Dens = 240, 240  
 [More Layer Comments below]



Notes: Pit dug to document snow conditions for research on PST geometry.. Additional Layer Comments: 36-40cm: Dens = 220, 230; 35-36cm: Thin crust of MF facets; 20-35cm: Dens = 190, 200; 20-35cm: Problematic layer;

377

378

379

380

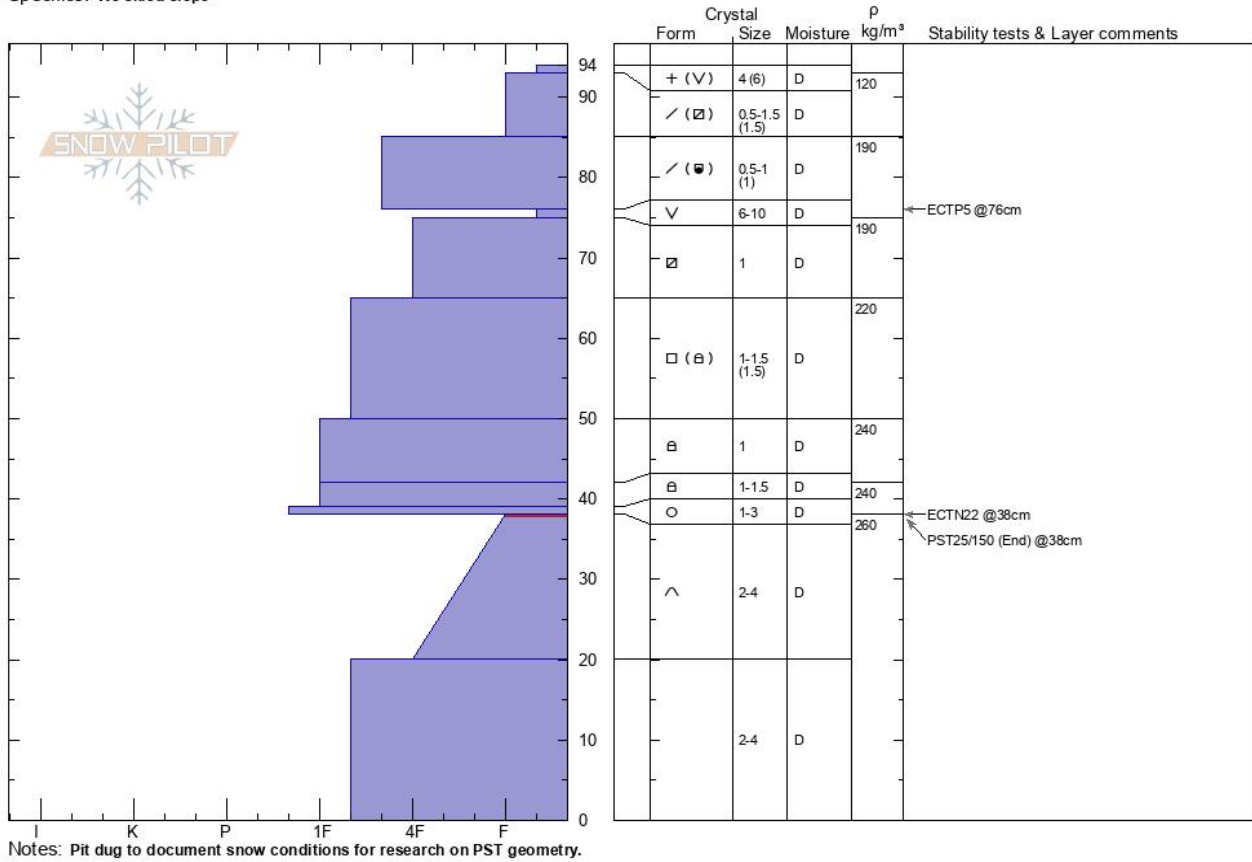
**Figure D2: Manual profile taken at the Bacon Rind field site on January 20<sup>th</sup> 2021. The blue area at the left site represents the hand hardness with snow height, On the right side, grain type, grain size, moisture and snow density are given. On the very right, stability test results are written at the height, of the tested weak layer.**



**Bacon Rind Sm Meadow** Karl Birkeland  
**Madison Range-S** 01/25/2021 - 12:00pm  
**MT** Co-ord: 44.84934N, -111.07942W  
 Elevation: 2321 m Slope Angle: 30°  
 Aspect: 80° Wind Loading:  
 Specifics: We skied slope

Stability:  
 Air Temperature:  
 Sky Cover: **CLR**  
 Precipitation: **NO**  
 Wind: **Calm**

HS: 94 Layer Notes:  
 38-20cm: Problematic layer



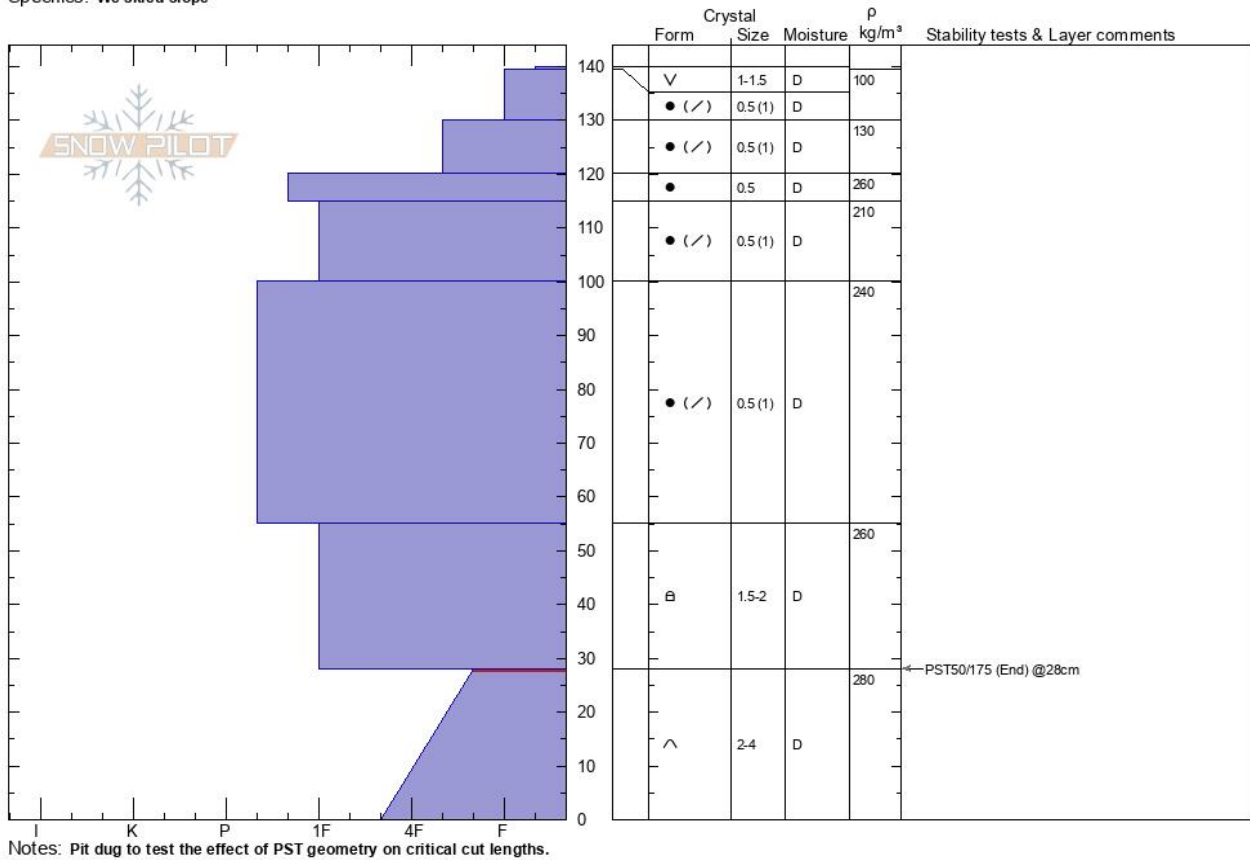
381  
 382 **Figure D3: Manual profile taken at the Bacon Rind field site on January 25<sup>th</sup>. The blue area at the left site represents the hand**  
 383 **hardness with snow height, On the right side, grain type, grain size, moisture and snow density are given. On the very right,**  
 384 **stability test results are written at the height, of the tested weak layer.**  
 385

**Mt Ellis**  
**Gallatin Range-N**  
**MT**  
 Elevation: **2439 m**  
 Aspect: **25°**  
 Specifics: **We skied slope**

**Karl Birkeland**  
**03/01/2021 - 12:00pm**  
 Co-ord: **45.58173N, -110.95616W**  
 Slope Angle: **27°**  
 Wind Loading:

Stability:  
 Air Temperature:  
 Sky Cover: **CLR**  
 Precipitation: **NO**  
 Wind: **Calm**

**HS: 140** Layer Notes:  
 28-0cm: **Problematic layer**



386

387 **Figure D4: Manual profile taken at the Mount Ellis field site on January 25<sup>th</sup>. The blue area at the left site represents the hand**  
 388 **hardness with snow height, On the right side, grain type, grain size, moisture and snow density are given. On the very right,**  
 389 **stability test results are written at the height, of the tested weak layer.**

390

391 **Competing interests**

392 The contact author has declared that none of the authors has any competing interests

393 **Acknowledgement**

394 We would like to thank Flavia Maeder, Erika Birkeland, and Alex Marienthal for assisting in the field. This research was  
 395 partly supported by the Swiss National Science Foundation (grant no. 200021\_169424) and funded by the Deutsche For-  
 396 schungsgemeinschaft (DFG, German Research Foundation) under grant no. 460195514.

- 398 Bair, E.H., Simenhois, R., van Herwijnen, A. and Birkeland, K., 2014. The influence of edge effects on crack propagation in snow stability  
399 tests. *The Cryosphere*, 8(4): 1407-1418.
- 400 Bair, E.H., Simenhois, R., van Herwijnen, A. and Birkeland, K.W., 2013. Edge effects in propagation tests. In: F. Naaim-Bouvet, Y. Durand  
401 and R. Lambert (Editors), *Proceedings ISSW 2013. International Snow Science Workshop, Grenoble, France, 7-11 October*  
402 *2013. ANENA, IRSTEA, Météo-France, Grenoble, France*, pp. 335-356.
- 403 Bergfeld, B., van Herwijnen, A., Bobillier, G., Larose, E., Moreau, L., Trottet, B., Gaume, J., Cathomen, J., Dual, J. and Schweizer, J.,  
404 2022. Crack propagation speeds in weak snowpack layers. *Journal of Glaciology*, 68(269): 557-570.
- 405 Bergfeld, B., van Herwijnen, A., Bobillier, G., Rosendahl, P.L., Weißgraeber, P., Adam, V., Dual, J. and Schweizer, J., 2023. Temporal  
406 evolution of crack propagation characteristics in a weak snowpack layer: conditions of crack arrest and sustained propagation.  
407 *Natural Hazards and Earth System Sciences*, 23(1): 293-315.
- 408 Bergfeld, B., van Herwijnen, A., Reuter, B., Bobillier, G., Dual, J. and Schweizer, J., 2021. Dynamic crack propagation in weak snowpack  
409 layers: insights from high-resolution, high-speed photography. *The Cryosphere*, 15(7): 3539-3553.
- 410 Birkeland, K.W., van Herwijnen, A., Reuter, B. and Bergfeld, B., 2019. Temporal changes in the mechanical properties of snow related to  
411 crack propagation after loading. *Cold Regions Science and Technology*, 159: 142-152.
- 412 CAA, 2016. *Technical Aspects of Snow Avalanche Risk Management—Resources and Guidelines for Avalanche Practitioners in Canada*,  
413 *Canadian Avalanche Association, Revelstoke, BC, Canada*.
- 414 Fierz, C., Armstrong, R.L., Durand, Y., Etchevers, P., Greene, E., McClung, D., Nishimura, K., Satyawali, P.K. and Sokratov, S., 2008.  
415 The 2008 international classification of seasonal snow on the ground. In: C. Campbell, S. Conger and P. Haegeli (Editors),  
416 *Proceedings ISSW 2008, International Snow Science Workshop, Whistler, Canada, 21-27 September 2008*, pp. 579-580.
- 417 Gaume, J., van Herwijnen, A., Chambon, G., Wever, N. and Schweizer, J., 2017. Snow fracture in relation to slab avalanche release:  
418 critical state for the onset of crack propagation. *The Cryosphere*, 11(1): 217-228.
- 419 Gauthier, D. and Jamieson, B., 2008a. Evaluation of a prototype field test for fracture and failure propagation propensity in weak snowpack  
420 layers. *Cold Regions Science and Technology*, 51(2-3): 87-97.
- 421 Gauthier, D. and Jamieson, B., 2008b. Fracture propagation propensity in relation to snow slab avalanche release: Validating the  
422 Propagation Saw Test. *Geophysical Research Letters*, 35(13): L13501.
- 423 Gauthier, D. and Jamieson, J.B., 2006a. Evaluating a prototype field test for weak layer fracture and failure propagation. In: J.A. Gleason  
424 (Editor), *Proceedings ISSW 2006. International Snow Science Workshop, Telluride CO, U.S.A., 1-6 October 2006*, pp. 107-116.
- 425 Gauthier, D. and Jamieson, J.B., 2006b. Towards a field test for fracture propagation propensity in weak snowpack layers. *Journal of*  
426 *Glaciology*, 52(176): 164-168.
- 427 Greene, E., Birkeland, K.W., Elder, K., McCammon, I., Staples, M., Sharaf, D., Trautman, S. and Wagner, W., 2022. *Snow, Weather, and*  
428 *Avalanches: Observation Guidelines for Avalanche Programs in the United States. American Avalanche Association, Denver*  
429 *CO, U.S.A.*, 110 pp.
- 430 Heierli, J., Gumbsch, P. and Zaiser, M., 2008. Anticrack nucleation as triggering mechanism for snow slab avalanches. *Science*,  
431 321(5886): 240-243.
- 432 Jamieson, J.B. and Johnston, C.D., 1998. Refinements to the stability index for skier-triggered dry slab avalanches. *Annals of Glaciology*,  
433 26: 296-302.
- 434 McClung, D.M., 2009. Dry snow slab quasi-brittle fracture initiation and verification from field tests. *Journal of Geophysical Research-*  
435 *Earth Surface*, 114: F01022.
- 436 Morin, S., Horton, S., Techel, F., Bavay, M., Coléou, C., Fierz, C., Gobiet, A., Hagenmuller, P., Lafaysse, M., Ližar, M., Mitterer, C., Monti,  
437 F., Müller, K., Olefs, M., Snook, J.S., van Herwijnen, A. and Vionnet, V., 2020. Application of physical snowpack models in  
438 support of operational avalanche hazard forecasting: A status report on current implementations and prospects for the future.  
439 *Cold Regions Science and Technology*, 170: 102910.
- 440 Richter, B., Schweizer, J., Rotach, M.W. and van Herwijnen, A., 2019. Validating modeled critical crack length for crack propagation in  
441 the snow cover model SNOWPACK. *The Cryosphere*, 13(12): 3353-3366.
- 442 Rosendahl, P.L. and Weissgraeber, P., 2020. Modeling snow slab avalanches caused by weak-layer failure - Part 1: Slabs on compliant  
443 and collapsible weak layers. *The Cryosphere*, 14(1): 115-130.
- 444 Schweizer, J., Reuter, B., van Herwijnen, A. and Gaume, J., 2016. Avalanche release 101. In: E. Greene (Editor), *Proceedings ISSW*  
445 *2016. International Snow Science Workshop, Breckenridge CO, U.S.A., 3-7 October 2016*, pp. 1-11.
- 446 Sigrist, C. and Schweizer, J., 2007. Critical energy release rates of weak snowpack layers determined in field experiments. *Geophysical*  
447 *Research Letters*, 34(3): L03502.
- 448 Simenhois, R. and Birkeland, K.W., 2008. The effect of changing slab thickness on fracture propagation. In: C. Campbell, S. Conger and  
449 P. Haegeli (Editors), *Proceedings ISSW 2008, International Snow Science Workshop, Whistler, Canada, 21-27 September*  
450 *2008*, pp. 755-760.
- 451 van Herwijnen, A., Gaume, J., Bair, E.H., Reuter, B., Birkeland, K.W. and Schweizer, J., 2016. Estimating the effective elastic modulus  
452 and specific fracture energy of snowpack layers from field experiments. *Journal of Glaciology*, 62(236): 997-1007.
- 453 Weißgraeber, P. and Rosendahl, P.L., 2023. A closed-form model for layered snow slabs. *The Cryosphere*, 17(4): 1475-1496.